Potential Cation and H^+ Binding Sites in Acid Sensing Ion Channel-1

Saher Afshan Shaikh and Emad Tajkhorshid
Department of Biochemistry, Beckman Institute, and Center for Biophysics and Computational Biology, University of Illinois at Urbana-Champaign, Urbana, Illinois 61801

ABSTRACT Acid sensing ion channels (ASICs) are cation-selective membrane channels activated by H^+ binding upon decrease in extracellular pH. It is known that Ca^{2+} plays an important modulatory role in ASIC gating, competing with the ligand (H^+) for its binding site(s). However, the H^+ or Ca^{2+} binding sites involved in gating and the gating mechanism are not fully known. We carried out a computational study to investigate potential cation and H^+ binding sites for ASIC1 via all-atom molecular dynamics simulations on five systems. The systems were designed to test the candidacy of some acid sensing residues proposed from experiment and to determine yet unknown ligand binding sites. The ion binding patterns reveal sites of cation (Na^+ and Ca^{2+}) localization where they may compete with protons and influence channel gating. The highest incidence of Ca^{2+} and Na^+ binding is observed at a highly acidic pocket on the protein surface. Also, Na^+ ions fill in an inner chamber that contains a ring of acidic residues and that is near the channel entrance; this site could possibly be a temporary reservoir involved in ion permeation. Some acidic residues were observed to orient and move significantly close together to bind Ca^{2+}, indicating the structural consequences of Ca^{2+} release from these sites. Local structural changes in the protein due to cation binding or ligand binding (protonation) are examined at the binding sites and discussed. This study provides structural and dynamic details to test hypotheses for the role of Ca^{2+} and Na^+ ions in the channel gating mechanism.

INTRODUCTION

Acid sensing ion channels (ASICs) are pH-sensitive cation channels belonging to the degenerin/epithelial (DEG/ENaC) sodium channel family (1–3). Four genes encode six ASIC isoforms (ASIC1a, ASIC1b, ASIC2a, ASIC2b, ASIC3, and ASIC4), which form homo- and heteromultimeric channels distributed in the mammalian central and peripheral nervous systems. These isoforms are characterized by their distinct pH dependence and desensitization kinetics (4,5). ASICs are known to be activated by H^+ binding upon a decrease in extracellular pH. However, the actual amino acid residues involved in H^+ binding and activation of these channels and the channel gating mechanism have yet to be fully determined.

ASIC activity is voltage independent but modulated by the concentration of extracellular Ca^{2+} (4,6,7). The role of Ca^{2+} in channel gating is rather intricate. It is known that increasing Ca^{2+} concentration decreases the amplitude of H^+ activated current, indicating that Ca^{2+} acts as an inhibitor for Na^+ permeation (6,7). Also, decreasing the Ca^{2+} concentration increases the apparent H^+ affinity for most ASIC channels, possibly because Ca^{2+} is bound to the acid sensing sites in the closed state of the channel (8). Yet, it has also been observed that ASIC3 requires micromolar concentrations of Ca^{2+} for activity (4). The mechanism of this modulation remains unclear. It has been proposed that the gating of ASIC1 involves the release of Ca^{2+} ions that block the channel pore through displacement by H^+ at low pH conditions (9). Subsequent studies have confirmed channel blocking by Ca^{2+} by identifying the Ca^{2+} binding residues responsible for the pore blockage as E425 and D432 (rat ASIC1a) in the transmembrane (TM) region (10), but delinked channel block by Ca^{2+} from channel opening due to H^+ binding (10,11). An allosteric mechanism was proposed whereby the displacement of Ca^{2+} by H^+ induces conformational changes linked to channel gating (11). Thus, a direct competition between Ca^{2+} and H^+ ions for some or all of the sites involved in channel gating is implicated; therefore, determining the putative ion and H^+ binding sites is important to allow a prediction of the ASIC1 gating mechanism.

Mutagenesis experiments have suggested particular residues that are important for H^+ sensing or gating, yet it has not been established whether any or all of these residues form the H^+ sensor. In one study (12), mutations were carried out in ASIC2a acidic residues absent in the H^+-insensitive splice variant ASIC2b, and the current measurements indicated five residues (H72, D77, E78, H109, and H180) whose substitution resulted in H^+ insensitivity. In another study (13), systematic mutations were used, and four residues (E63, D78, H72, and H73) in rat ASIC1a were pinpointed, whose substitution in double or triple mutant systems resulted in H^+ insensitivity of the channel. In at least two mutagenesis studies conducted after the structure of ASIC1 was obtained, mutations were introduced in some acidic residues proposed to be acid sensing sites because their structural arrangement suggested that they exist as carboxyl-carboxylate pairs (13,14). In both studies, it was concluded that, although mutation of some of these acidic residues (namely, D346 and D350 in chicken ASIC1 (14) and E219, D237, and E238 in rat ASIC1 (13)) resulted in reduced H^+ affinity of the channel, the mutation(s) did not fully abolish H^+ sensing. These results suggest that other residues also participate in the H^+ sensing

Submitted July 3, 2008, and accepted for publication August 20, 2008.

Address reprint requests to Emad Tajkhorshid; Tel.: 217-244-6914; Fax: 217-244-6078; E-mail: emad@life.uiuc.edu.

Editor: Richard W. Aldrich.

0006-3495/08/12/5153/12 $2.00

doi: 10.1529/biophysj.108.141606

mechanism. It has been proposed that the H^+ sensor may be composed of multiple sites distributed over the structure and that the above-mentioned studies have characterized only some of these. Thus, it has not been established if all of the binding sites have been determined.

The recently solved crystal structure of chicken ASIC1 reveals a homotrimer with a particularly notable pocket on the surface containing several acidic residues at the interfaces of the monomers, which have been shown, at least partially, to participate in H^+ sensing (13,14). Acid sensing occurs on the extracellular domain with an apparent pH_{50} of 5.9, 5.0, and 5.4 for rat ASIC1a, ASIC2a, and ASIC3, respectively. Histidine, aspartate, and glutamate residues are likely candidates to respond to a change in pH that is in the range for ASIC activation. The ASIC1 crystal structure carries a high overall negative charge (−52), with 176 acidic (D and E), 124 basic (K and R), and 15 histidine residues distributed on the surface and in some parts of the protein interior. The structure thus contains several possible H^+ or cation binding sites, necessitating systematic studies in which the actual sites could be pinpointed.

We have adopted a computational approach for the identification of cation binding sites on a protein from the ion binding patterns obtained through simulations. Applying this methodology to ASIC1, we have investigated putative cation and H^+ binding sites in a series of ASIC1 simulations. Differential effects of change in protonation states of particular residues and of the nature of ions on ion localization and the structural consequences were also observed. The calculations were carried out with an explicit, all-atom representation of membrane, water, ions, and the protein using classical molecular dynamics simulations (each with a duration of 30–50 ns). To our knowledge, this study represents the first description of the dynamics of ion binding and its structural effects on the ASIC system.

Our results reveal cation localization at possible acid sensing sites. Under the dynamic simulation environment, the structure exhibits local conformational changes that are probably influenced by the presence of bound ligand (H^+) or cation(s). Building on the results obtained for cation binding and associated structural changes, we propose the possible residues involved in H^+ or Ca^{2+} binding in ASICs. A few of the proposed sites are consistent with results from experimental mutagenesis studies. The results also demonstrate some novel potential cation binding sites that have not been characterized in previous studies.

METHODS

System design

In the ASIC1 crystal structure, eight acidic residues in each monomer are located in such a manner that they form four individual pairs (D238:D350, E239:D346, E220:D408, and E80:E417). The pairs are held by carboxyl-carboxylate interactions; in other words, at least one residue of each pair should be protonated to retain this spatial arrangement (14). Because the crystal structure is reported to be in the *desensitized* state, which is the ligand-bound state, the systems in this study were designed with the consideration that these four pairs (totaling 12 pairs in the trimer) could possibly be acid sensing sites. Simulation systems 1 through 4 (Table 1) were designed to vary the protonation states of these four pairs so that the structural effects of protonation/deprotonation and the cation binding ability of these residues could be probed. In system 1, all four pairs in the first monomer were charged; in the second monomer, these pairs were uncharged; and, in the third monomer, each pair had one charged and one uncharged residue. Systems 2 through 4 were then designed as an extension of system 1. In system 2, all four pairs were charged in all three monomers; in system 3, all four pairs were uncharged in all three monomers; and, in system 4, all four pairs were charged-uncharged combinations. Na^+ was chosen as the counterion for systems 1 through 4 for two reasons: 1), it was expected that Na^+ binding at certain sites on the protein could hint at the possible residues involved in its passage through the channel and Na^+ selectivity; and 2), Na^+ binding could reveal sites where H^+ ions could bind and activate the channel. Keeping in view that the fully uncharged (system 3) or charged-uncharged pairs (system 4) would have favorable interactions within the ion pairs and so remain structurally close to the desensitized (crystal) state, it could be conjectured that the all-charged pairs in which the ligand (H^+) is not bound could represent a state closer to the inactive Ca^{2+}-bound form. System 5 was then designed using Ca^{2+} as the

TABLE 1 Summary of the five simulation systems

System	Cationic concentration (mM)	D238:D350	E239:D346	E220:E408	E80:E417	Other protonated residues	Comments	Simulation length (ns)
1	~35 (Na^+)	p–p:– –p	p–p:– –p	p–p:– –p	– –p:p–p	H74, H111 E98,E243,E255,E354	4 acidic residue pairs in different protonation states in the 3 monomers	50
2	~140 (Na^+)	– – –:– – –	– – –:– – –	– – –:– – –	– – –:– – –	H74, H111	All acidic residues charged (deprotonated)	50
3	~100 (Na^+)	ppp:ppp	ppp:ppp	ppp:ppp	ppp:ppp	H74, H111	4 acidic residue pairs uncharged (protonated)	30
4	~120 (Na^+)	ppp:– – –	ppp:– – –	ppp:– – –	– – –:ppp	H74, H111 E98,E243,E255,E354	4 acidic residue pairs as charged/uncharged pairs	30
5	~50 (Ca^{2+})	– – –:– – –	– – –:– – –	– – –:– – –	– – –:– – –	H74, H111	All acidic residues charged (deprotonated)	50

The cation concentration, protonation states of particular residues, and simulation lengths are listed. The cationic concentration is calculated only in the solution compartments of the simulations. p, residue protonated in a monomer; ppp, residue protonated in all three monomers; (–), residue deprotonated in a monomer; (– – –), residue deprotonated in all three monomers.

counterion and keeping all four pairs charged, assuming it to be the relaxed, closed state of the channel where it binds Ca^{2+} to be subsequently displaced by H^+ for channel activation. Details of the setup for each system are described below.

System setup

The recently solved high-resolution crystal structure of chicken ΔASIC1 (Protein Data Bank (PDB) code 2QTS) (14) was used as a starting point for all the simulations. It may be noted here that the reported structure has residues missing at the N- and C-termini, which are both located on the cytosolic side. Because this study is focused mainly on the extracellular region and ion binding sites, the missing residues are not expected to affect the results. Bound Cl^- ions reported in the crystal structure were retained. Detergent molecules were removed, and the protein was embedded in a POPC membrane (110×110 Å^2, 338 lipid molecules), generated using the Membrane Builder module of visual molecular dynamics (VMD) software.

pKa calculation on the structure with PROPKA software (15) was used to determine the optimal titration states of acidic residues and histidines at a pH of 7.0. Five systems were designed with combinations of protonation states of these residues (Table 1), and hydrogen atoms were added accordingly using the psfgen plugin in VMD (16) with CHARMM27 (17) topology files. The protein has an overall charge of -22 to -30 depending on the assigned protonation states. The cionize program in VMD (18), which places ions based on the Coulombic potential calculated for the protein, was used. Keeping a minimum ion-ion and ion-protein distance of 5 Å each, the maximum number of cations (Na^+ in systems 1–4 and Ca^{2+} in system 5) that could be placed near the protein surface was added to the systems.

In system 1, Na^+ ions were added only for neutralization, resulting in a $[Na^+]$ of ~35 mM, which is low with respect to physiological concentration and could result in undersampling of ion binding events. This potential problem was remedied in systems 2 through 4 in which additional Na^+ and Cl^- ions were added to the systems, thus taking $[Na^+]$ to ~100–140 mM, which corresponds to physiological concentrations. After the Coulombic potential-based ion addition, system 5 had a very high $[Ca^{2+}]$ of ~50 mM compared to the physiological concentration; hence, only Cl^- ions were added for neutralization. The high $[Ca^{2+}]$ would increase the probability of binding events in the simulation, thus allowing better sampling within the simulation timescale. This increased $[Ca^{2+}]$ could, however, also result in oversampling at the Ca^{2+} binding sites, a point that has been considered in the interpretation of the results.

Crystal water molecules and those molecules associated with the lipids were retained, and more water molecules were added on both sides of the membrane, with the solvent layer extending up to ≤10 Å from the protein surface to ensure adequate solvation of the system. Each simulation system thus constructed contained ~180,000 atoms. Fig. 1 shows the system setup, and Table 1 summarizes the system details for each setup.

Simulation protocol

All simulations were performed using NAMD 2.6 (19), adopting periodic boundary conditions with a time step of 1 fs. The CHARMM27 force field (17) with ϕ/ψ cross-term map corrections (20) was used for describing proteins, lipids, and ions, whereas the TIP3P model was used for water (21). Short-range, nonbonded interactions were calculated using a cutoff distance of 12 Å, and long-range electrostatic interactions were calculated using the particle mesh Ewald method (22). Lipid tails were first melted for 1 ns in NP_nT conditions (constant number of particles, pressure normal to the membrane, and temperature) in which all atoms of the protein and the heavy atoms of the lipid headgroups were constrained using harmonic potentials ($k = 7$ kcal/mol/Å^2). A constant temperature of 310 K was maintained by using Langevin dynamics with a damping coefficient of 1 ps^{-1}, whereas the Langevin piston method (23,24) was used to maintain a constant pressure of 1.0 atm with a piston period of 100 fs. Next, constraints on the lipid headgroups were removed, and the system was further equilibrated for 1 ns to allow for packing of the lipid molecules around the protein. After these steps, all constraints were removed, the area of the lipid bilayer was allowed to be flexible at NPT (constant number of particles, constant pressure, and constant temperature) conditions, and equilibration was continued for an additional 0.5 ns. Finally, the production runs were carried out with a constant area of the lipid bilayer in the NP_nT (constant pressure only along the membrane normal) ensemble and with a constant pressure of 1 atm along the membrane normal for 30 to 50 ns each.

Analytical procedure

Identifying persistent ion binding events

To distinguish between incidental and persistent binding residues, we adopted a cutoff of ion binding for >50% of the simulation time in the three 50 ns simulations (systems 1, 2, and 5) and >30% in the two 30 ns simulations. The latter cutoff is more relaxed than the former to compensate for the shorter duration (30 ns) of these two simulations. A residue was considered to have bound a cation whenever the ion occurred within a cutoff distance of 5.5 Å from its side chain. This cutoff was adopted to encompass all significant protein-cation binding events. It was determined based on the protein-cation radial pair distribution function (Fig. 2), which indicates that, for Ca^{2+} and Na^+ ions, most contacts with the protein are between 2.00 and 2.75 Å, with some between 4.00 and 5.00 Å. Cation binding for each residue in all three monomers was monitored throughout the trajectories with an evaluation at every 100 ps. The three monomers are identical in sequence and almost so in structure, and we observed that they showed similar behaviors in cation binding at many —but not all — sites at different points of time. Although the probability of cation binding to any of the monomers is the same when averaged over time, making this observation for all binding sites would require a longer equilibration time. Hence, to ensure that no residues that can bind cations persistently were neglected, a binding event was counted even if it occurred for a residue in only one monomer. The residues thus determined are shown in Fig. 4 *a*.

Determining cation binding pairs

Assuming that H^+ binding induces some conformational changes to effect ASIC gating, it seems plausible that displacement of cations bound by more than one residue would result in more noticeable conformational changes than for single residues. Hence, the residues filtered as described above were analyzed to obtain residue pairs that bind cations. Cation binding pairs were initially determined using two criteria: 1), the carboxyl or hydroxyl groups of the two side chains forming the pair must lie within 7 Å; and 2), the cation must lie within 5.5 Å of these groups on both the amino acids. Analysis of the trajectories from systems 2 and 5 was considered sufficient because they represent the Na^+ and Ca^{2+} systems and demonstrate ion binding at residues in systems 1, 3, and 5 to either the same or an even greater extent. The analysis returned several possible combinations of pairs in each case, and so two additional criteria were applied to sift the results and obtain the most relevant pairs. First, our earlier cutoff of ion binding for >50% of the simulation time was applied. Second, in the case of clusters of residues in which more than one combination was possible, residue pairs that were aligned most optimally for ion binding (for example, carboxyl or hydroxyl groups from both partners fully participating in ion binding) were chosen over side-by-side binding pairs whenever necessary. The 10 pairs thus obtained are shown in Fig. 4 *b*.

Monitoring cation binding for chosen binding pairs

For each of the pairs obtained above, the number of bound cations was determined throughout the simulation. The cutoff distance of 5.5 Å used earlier was adopted. The number of cations within 5.5 Å of the carboxyl side chain or the hydroxyl groups of each amino acid forming the pair was counted. This evaluation was carried out for all three monomers throughout the five simulation trajectories at every 10 ps. The binding patterns obtained are presented in Fig. 4 *c* and discussed in the next section.

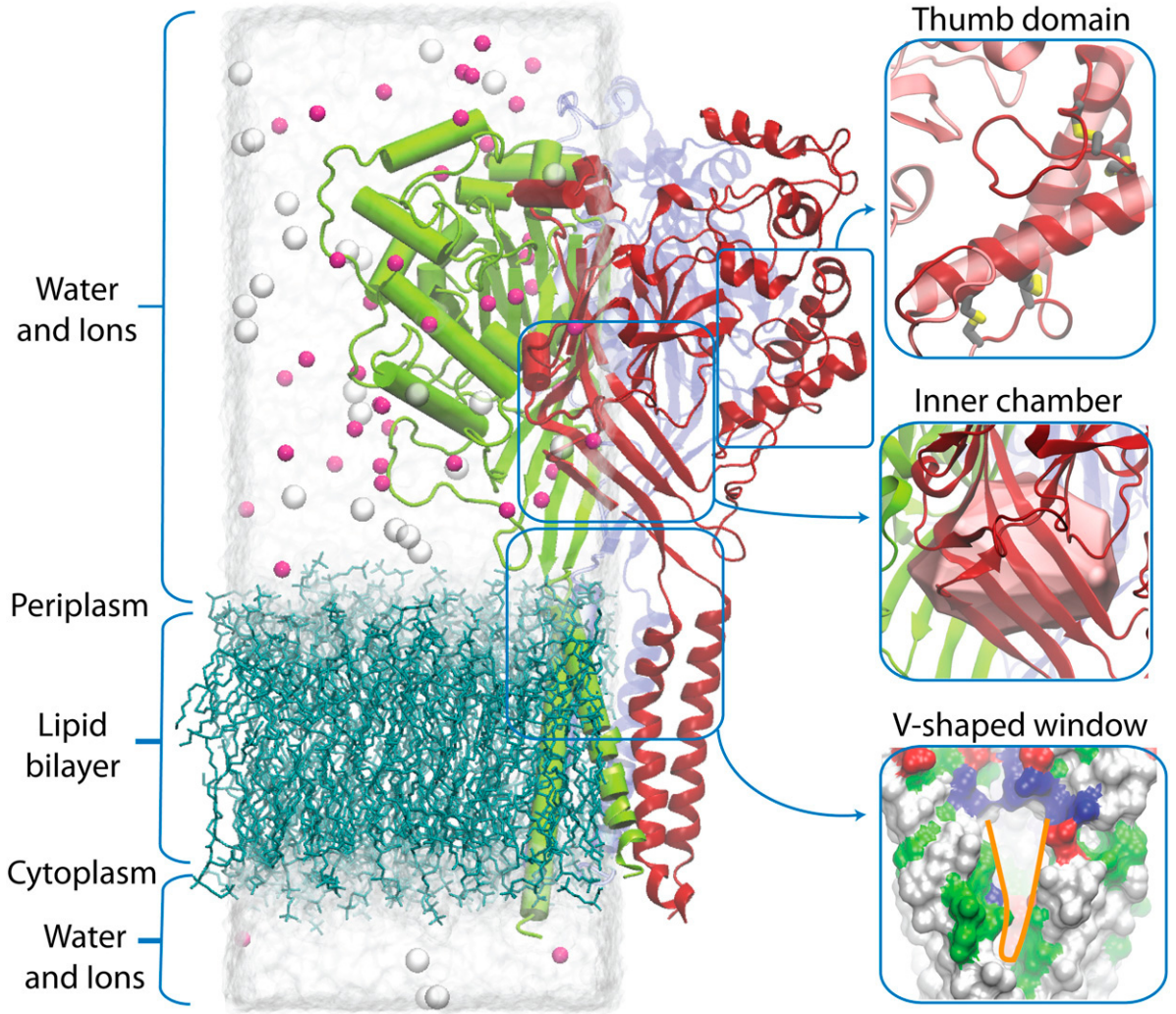

FIGURE 1 The ASIC1 simulation system. The left panel shows the system setup for ASIC1 embedded in a POPC lipid bilayer and surrounded by explicit water and counterions Na^+ (*pink*) and Cl^- (*white*). The three monomers in the protein are colored in red, green, and blue, respectively. The right panel shows three important regions discussed in this study: the thumb domain (*top*), which is mainly composed of two connected helices, is shown in red along with its four disulphide bonds in yellow; the inner chamber (*middle*), an acidic cavity enclosed by β-sheets is highlighted using a surface representation; the V-shaped window (*bottom*) at the interface of two monomers near the start of the TM region is highlighted in orange. The V-shaped window is shown in a surface representation where amino acids are colored according to polarity and charge (negatively charged (*red*), positively charged (*blue*), polar (*green*), and nonpolar (*white*)).

In a separate analysis performed to determine the ligand atoms in the first coordination shell of the protein-bound cations, a more stringent cutoff of 2.5 Å between oxygen atoms and the bound cation was used. Here, a cation was considered protein-bound if it was within 5.5 Å of at least two oxygen atoms of the protein and within 2.5 Å of at least one of them. The numbers of oxygen atoms from water, protein backbone, and protein side chains within 2.5 Å (that is, directly contributing to the coordination shell) of the protein-bound cations were then determined. This analysis was carried out on simulation system 2 for Na^+ and system 5 for Ca^{2+}. The average numbers of coordinating oxygen atoms are reported in Table 2.

RESULTS AND DISCUSSION

In this study, ion dynamics were monitored during simulations with the aim of determining putative acid sensing or Ca^{2+} binding/displacement sites. Structural analyses were also conducted to determine the effects of protonation or cation binding on the ASIC1 structure. Plots of the root mean-square deviation (RMSD) of the protein backbone from the starting structure show some deviation from the crystal structure in all systems when allowed to equilibrate in solution, with the sharpest RMSD changes occurring within the first 5 ns (Fig. 3 *a*). The maxima in plots of residue-wise RMSDs averaged over the last 1 ns in each simulation (Fig. 3 *b*) indicate that major contributions to the deviations arise from movement at the following regions: residues 45–65 and 425–455 (TM region); residues 105–160 (mainly forming the so-called ''finger'' domain (14) located at the upper, outer side of each monomer); residues 200–220 (loop region);

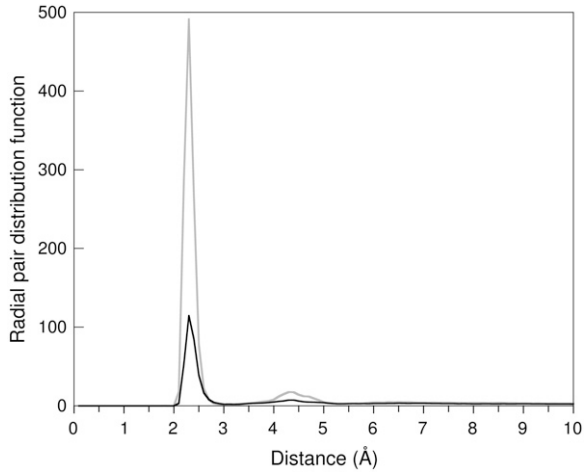

FIGURE 2 Radial pair distribution function of Na^+ protein (*black*) and Ca^{2+} protein (*gray*) systems determined over the full trajectories for system 2 and 5. Although cations mostly reside between 2 and 2.75 Å of carboxylic groups, they also show a presence between 4 and 5 Å; hence, a cutoff of 5.5 Å was chosen to determine cation binding.

residues 280–305 (loop region); and, in two systems, residues 325–360 (''thumb'' domain and associated loop (Fig. 1)). Structural deviations occurring specifically at the binding sites were also measured and are discussed in detail in the following sections.

The crystal structure of ASIC1 (14) shows a significant asymmetry in its TM domains, a feature most likely arising from crystal packing effects. Deviations in the TM region from the crystal structure occur during the simulations primarily due to a change in the relative orientation of the TM helical bundle with respect to the extracellular domain. However, the individual TM helices remain asymmetric, as in the starting crystal structure, within the timescale of these simulations.

Although this study is focused on cation binding sites, the dynamics of the three bound Cl^- ions reported in the ASIC1 crystal structure were also monitored to examine their behavior when putative acid sensing sites on the protein are protonated/deprotonated. In all simulations, at least one Cl^- leaves its binding site, which is then occupied by water, and the Cl^- ions do not reenter the site. In system 3, where many acidic residues are uncharged, two Cl^- ions leave, of which one interestingly takes a route through the acidic pocket. In system 4, all three bound Cl^- ions leave, although the negative charge on the protein is lower compared to systems 2 and 5 in which only one Cl^- ion leaves. Our results, therefore, do not provide any evidence of a direct correlation between the retention of the bound Cl^- ions in their binding site and the protonation state of putative acid sensing residues.

An inspection of the first coordination shell of cations bound closely at the putative binding sites reveals that, on average, the number of oxygen atoms coordinating protein-bound Na^+ ions is ~5, whereas the number of atoms coordinating protein-bound Ca^{2+} is ~7 during the simulations (Table 2). The backbone oxygen atoms seem to rarely participate in the coordination, and both cations on average continue to interact more with water molecules even after binding to the protein (see Fig. S1 in Supplementary Material, Data S1). From these observations, it appears that the protein does not offer very tight binding sites for the cations, possibly to allow a ready displacement of the bound cations by H^+ for acid sensing.

The five simulations undertaken in this study represent unique systems with differences in protonation states of key acidic residues, type of cation, or ionic concentration (Table 1) as described in Methods. This allows a comparison of the systems to determine common characteristics among all of them and unique features of specific systems as discussed below.

Acidic pocket residue pairs emerge as strong candidates for the H^+ sensor

Residue pairs D238:D350, E239:D346, and E220:D408 are located in three surface cavities (one each at the monomer interfaces (Fig. 4 *b*)), contributing to the highly negative potential (14) in these cavities, hereby referred to as the *acidic pockets*. Several other charged and polar residues are

TABLE 2 The coordination numbers of protein-bound Na^+ (Na^+ c.n.) and Ca^{2+} (Ca^{2+} c.n.) ions at the 10 cation binding sites (Fig. 4 *b*), determined as the number of oxygen atoms within the first coordination shell (2.5 Å) of the ion, averaged over the frames in which a protein-bound ion existed

Cation-Ligand	D238:D350	E239:D346	E220:D408	E80:E417	E339:E343	D132:E133	D127:E236	E299:D332	D290:E363	E451:D454
Na^+ c.n.	4.7	4.7	4.7	4.6	4.6	4.6	3.3	4.4	4.6	4.5
Na^+-O:water	3.0	2.6	2.3	2.0	2.8	3.2	2.3	3.0	2.7	3.0
Na^+-O:protein backbone	0.0	0.0	0.2	0.4	0.0	0.2	0.3	0.0	0.3	0.0
Na^+-O:protein side chain	1.7	2.1	2.2	2.2	1.8	1.2	0.7	1.4	1.6	1.5
Ca^{2+} c.n.	6.6	6.9	6.3	7.0	6.6	7.2	7.0	7.0	6.8	7.0
Ca^{2+}-O:water	4.0	4.9	4.2	5.0	4.0	3.9	3.9	3.8	4.8	5.0
Ca^{2+}-O:protein backbone	0.0	0.0	0.3	0.0	0.0	0.0	0.0	0.0	0.0	0.0
Ca^{2+}-O:protein side chain	2.6	2.0	1.8	2.0	2.6	3.3	3.1	3.2	2.0	2.0

The data reported is for system 2 for Na^+ and system 5 for Ca^{2+}. Na^+(/Ca^{2+})-O:water refers to the average number of liganding oxygen atoms from water; Na^+(/Ca^{2+})-O:protein backbone and Na^+(/Ca^{2+})-O:protein side chain refer to the average number of oxygen atoms from the protein backbone and side chain, respectively.

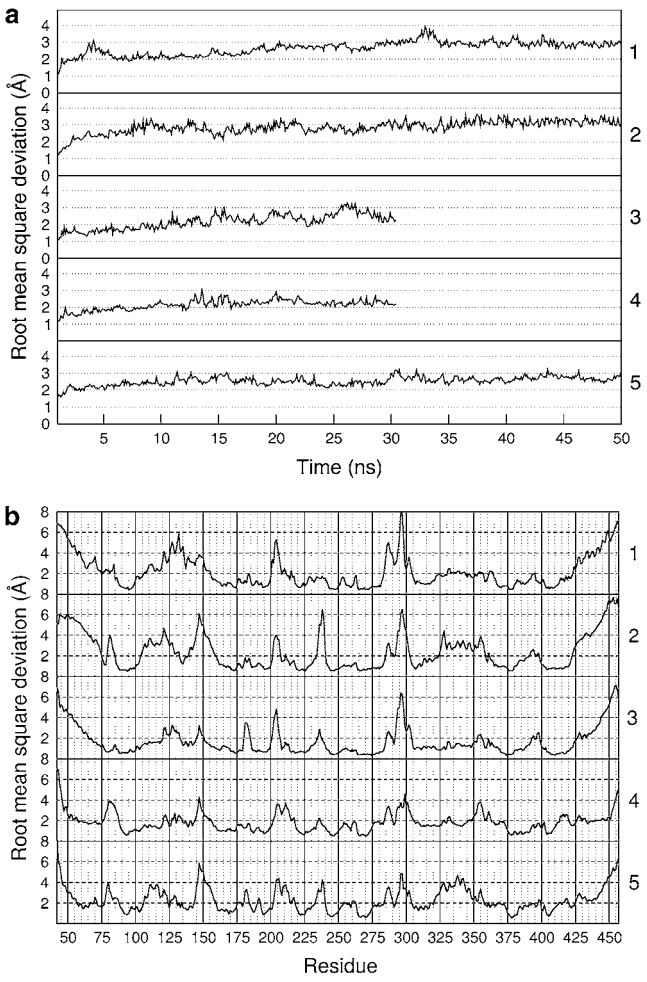

FIGURE 3 (*a*) RMSD of the protein backbone from the starting structure for the five systems (numbered *1–5*) as a function of simulation time. The greatest change of RMSD occurs within the first 5 ns. (*b*) Residue-wise average RMSD calculated for the backbone heavy atoms of all residues in the five systems. Deviations from the structure at the start of the simulation, are averaged over the last 1 ns of each trajectory. Comparison reveals the difference in mobility of residues under different conditions across the five systems.

also present in these acidic pockets; notable among these are the acidic E98, E243, D260, and E354; the basic R191; and the polar Y192, T215, T240, S241, and Q271 residues that interact with the ions bound in the acidic pockets as demonstrated in our simulations (Fig. 4 *a*).

Different protonation states of the residues in the three pairs D238:D350, E239:D346, and E220:D408 are adopted in systems 1 through 5 in which these states are present as all-charged, all-uncharged, or charged-uncharged pairs. Fig. 4 *c*, columns A–C, shows the number of cations binding at these three pairs. System 1 cation binding data indicate notable Na^+ binding only at D238:D350 and E220:D408 and some binding at E239:D346. System 2, which contains all-charged pairs, demonstrates more extensive ion binding, with several instances of more than one cation bound at a pair and binding at E239:D346. System 3, where these pairs are uncharged, shows negligible Na^+ binding, which is expected due to the neutral residues. System 4 contains charged-uncharged pairs and, although it cannot attract cations as strongly as the all-charged system 2, it shows appreciable ion binding at D238:D350, which is the most accessible pair, and some binding at the lesser accessible E220:D408 pair. System 5 cation binding data indicate continuous binding of Ca^{2+} at all three pairs, where each pair is always occupied by Ca^{2+} in at least one monomer. Comparing these systems (Fig. 4 *c*), it is observed that. when the ligand (H^+) is fully bound at these sites, as in system 3, cation binding is fully inhibited; when it is bound to half the residues of these pairs as in system 4, cation binding is significantly inhibited. Thus. it appears that Ca^{2+} or Na^+ binding occurs appreciably in the acidic pocket only when all residues in the D238:D350, E239:D346, and E220:D408 pairs are charged and that ligand (H^+) binding inhibits cation binding at these sites.

The residue-wise RMSD data for these three pairs (Fig. 5 *a*, *columns A–C*) show several interesting features. The most notable feature is a large deviation of D238 (of D238:D350) and the E239:D346 pair away from the starting structure in the two all-charged systems 2 and 5 (Fig. 5 *b*). D238 and E239 reside on a loop that moves away, presumably due to repulsion, in the two all-charged systems, thus making the E239:D346 pair more accessible; hence, significant cation binding is observed at this pair in only these two systems. Interestingly, the RMSDs are smaller for the Ca^{2+} system than the Na^+ system, suggesting that a single Ca^{2+} provides better screening between two charged, acidic amino acids than when possibly more than one Na^+ is present. Although the deviation remains small in systems 1, 3, and 4, system 3 shows the least deviation, probably because uncharged pairs are favored over charged-uncharged pairs at this location because of the negative potential that is developed due to several other acidic groups in this pocket. The E220:D408 pair shows very little deviation in all systems, possibly because both are rigidified by the β-sheet on which they are present. This rigidity reduces the chance of this pair participating in any conformational change associated with acid sensing or cation binding/dissociation.

Based on these observations, it may be hypothesized that, if the resting, Ca^{2+}-bound state is all-charged (as in system 5), then Ca^{2+} displacement by the ligand (H^+) could cause conformational changes involving the D238- and E239-containing loop. These changes could take the structure near to the desensitized ligand-bound form (as in systems 3 and 4), which might be structurally similar in this region to the open, ligand-bound form.

Previous experimental studies have reported that the mutation of residues D346 and D350 in chicken ASIC1 (14) and of residues equivalent to E220 and E239 in rat ASIC1 (13) decreases acid-activated currents. This fact, coupled with the observed features in our simulations (that is, persistent cation binding and significant structural differences in the ligand (H^+)-bound, cation-free state versus the ligand-free, cation-

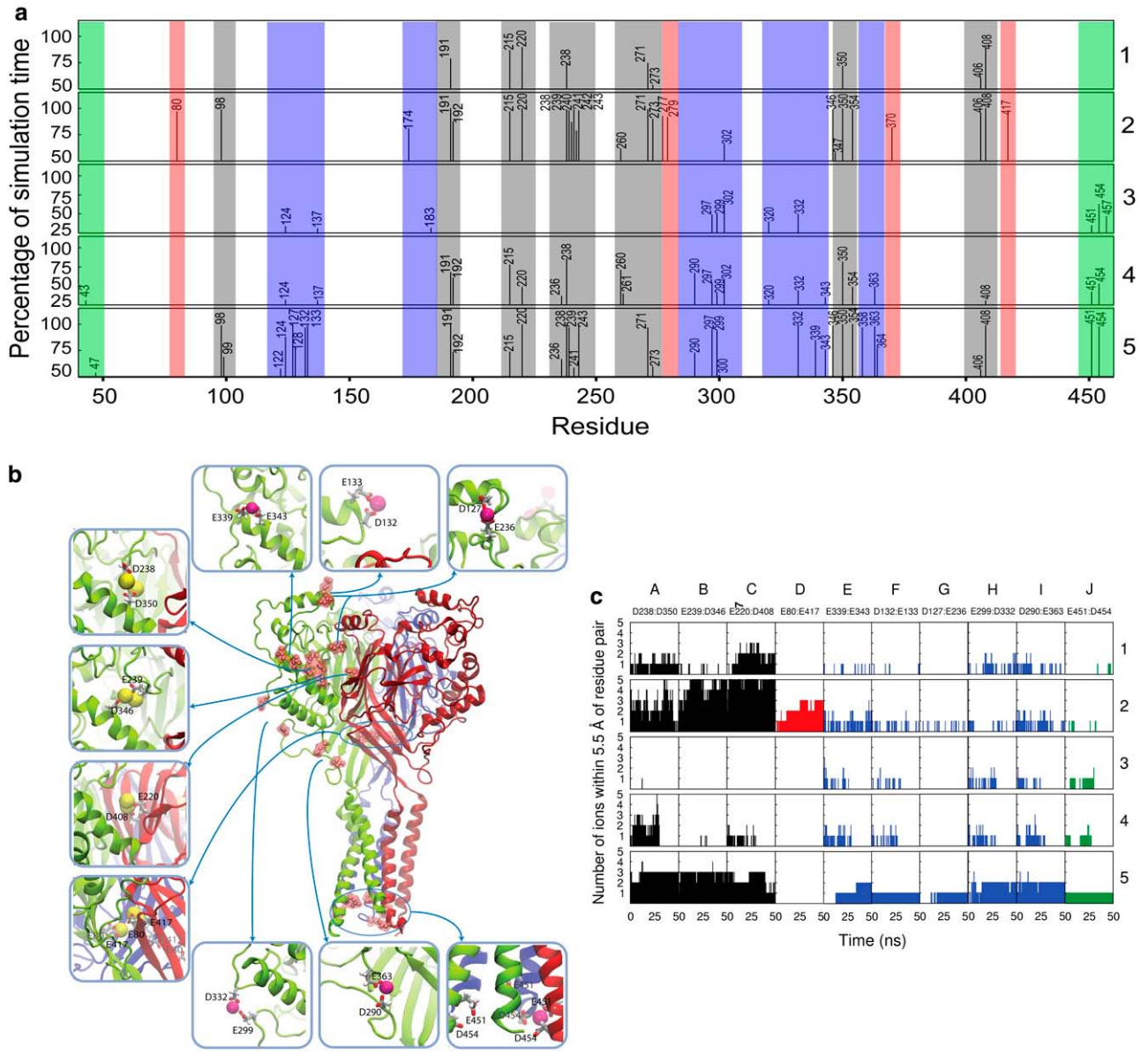

FIGURE 4 (*a*) Residues from any monomer binding at least one cation between 50 and 100% of the simulation time in 50 ns simulations (systems 1, 2, and 5) and between 30 and 100% of the simulation time in the 30 ns simulations (systems 2 and 3). Each residue is represented as a bar labeled by its residue number, with the bar height representing the percentage of simulation time when a cation is bound to it. Regions to which these residues belong are color-coded: acidic pocket (*gray*), inner chamber (*red*), surface residues (*blue*), and TM (*green*). (*b*) The 10 residue pairs revealed to be potential Ca^{2+} and/or H^{+} binding sites, and their location on the ASIC1 trimeric structure. For clarity, all pairs except two (E80:E417 and E451:D454) are shown on only one monomer. The full-length figure represents the starting structure and is close to the crystal structure. Close-up snapshots represent actual binding events taken from the trajectories of system 2 (with Na^{+} in *yellow*) and system 5 (with Ca^{2+} in *pink*). Residues forming the pair are labeled with their residue number. (*c*) Number of cations binding at the 10 residue pairs forming possible binding sites for Ca^{2+} or H^{+}. Each column (*A–J*) corresponds to a residue pair, and each row (*1–5*) corresponds to a simulation system. Regions to which these residues belong are color-coded like in (*a*). Whereas sites A–C are well populated in most systems, site D is populated only in system 2, and sites E–J are persistently populated mainly in system 5. An enlarged version of panel *b* is shown in Data S1.

bound state) support D238:D350 and E239:D346 as strong candidates for acid (H^{+}) sensing sites.

Curious site in protein interior (inner chamber)

The residue pair E80:E417 participates from each monomer to form a ring of acidic residues in an inner cavity of the protein (hereby referred to as ''inner chamber'' or ''chamber'') in a region just above the mouth of the TM pore (Fig. 4 *b*). Several other polar residues also participate in this site, notably Q277 and Q279, which interact with the ions bound at this site (Fig. 4 *a*). The protonation states of E80 and E417 are also varied along with the previously discussed three pairs in the acidic pocket (Table 1). The all-charged, Na^{+} system (system 2) shows a striking difference from all the other

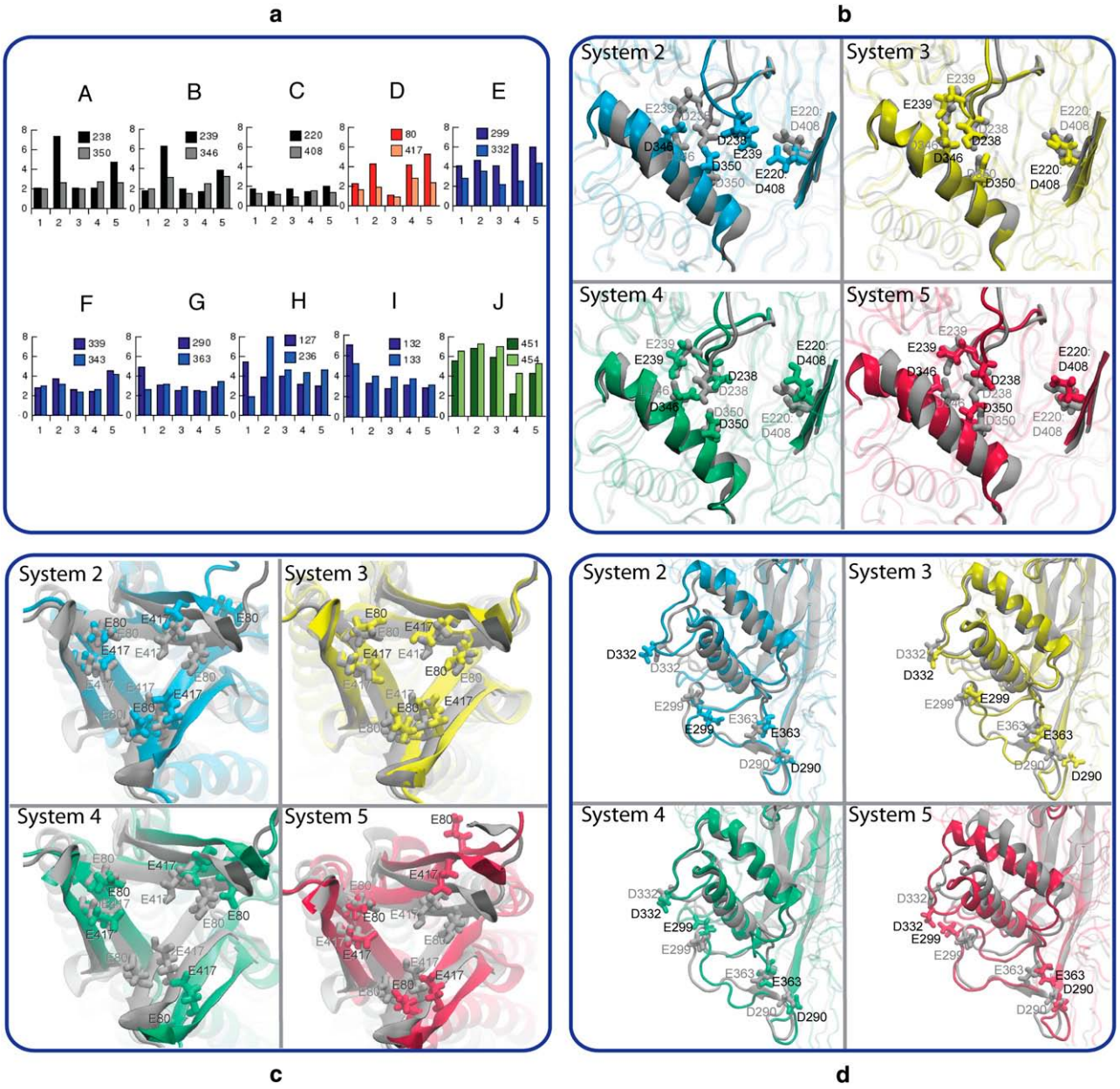

FIGURE 5 (*a*) Residue-wise average RMSD for each of the 20 residues forming the 10 putative Ca^{2+} and/or H^{+} binding pairs (*A–J*). Deviations from the starting structure are averaged over the last 1 ns of each trajectory. (*b–d*) Snapshots obtained at the end of simulations of systems 2, 3, 4, and 5 (in *color*) superimposed upon the starting structure (*gray*). The extent of structural deviation during the simulations is illustrated. (*b*) Acid pocket residues: The all-charged, Na^{+} system 2 shows large movement of the D238-E239 containing loop and some translation of the D346-D350 containing helix; all-uncharged system 3 shows minimum deviation; charged-uncharged system 4 also shows only minor deviation; all-charged Ca^{2+} system 5 shows some deviation in the D346-D350 containing helix but much lesser overall deviation than system 2. (*c*) Inner chamber residues: In system 2, filling of Na^{+} ions (not shown) reverses the cavity widening caused by charged group repulsions, and E80 of one chain flips out; system 3 shows minimum deviation; system 4 shows cavity widening; system 5 shows cavity widening, and E80 of one chain flips out. (*d*) Ca^{2+} binding surface residues, D290:E363 and E299:D332 pairs: System 2 shows some deviation of the thumb domain but does not exhibit D290:E363 and E299:D332 pair formation; systems 3 and 4 show very minor deviation; system 5 shows that D290:E363 and E299:D332 residues move together to form Ca^{2+} binding pairs, and a noticeable slanting of the thumb domain occurs. Enlarged versions of panels *b–d* are shown in Data S1.

systems by exhibiting an accumulation of Na^{+} ions in this inner chamber as shown in Fig. 4 *c*, column D. As the simulation starts, the chamber first widens, presumably due to repulsion among these residues, and E80 of one of the monomers flips out slightly, making the chamber accessible to the outer environment. Within 5 ns, the site starts filling with Na^{+} ions moving in, as if they are ushered in by the E80 facing outward; surprisingly, as the simulation proceeds, 3 Na^{+} ions occupy this relatively small cavity, accompanied by a narrowing of the chamber.

None of the other systems shows any ions entering this site. In systems 1, 3, and 4, this finding is probably because the chamber does not present a strong enough negative potential to attract ions inside, because the ring formed by three E80:E417 pairs is either partially or fully uncharged. System 5 would be expected to show a similar behavior because it is an all-charged system but, surprisingly, does not. This interesting difference between the Na^+ system (system 2) and the Ca^{2+} system (system 5) can be attributed to two reasons. First, the positively charged residues near the inner chamber entrance, notably R85, provide a strong electrostatic barrier to the doubly charged Ca^{2+} ion. Second, the cation seems trapped by acidic residues near the chamber entrance, especially E363 and D290 (Fig. 4 *b*), which bind the cation strongly and do not allow it to move further during the simulation. These interactions might present a means of selectivity that allows Na^+ ions to enter the chamber but not Ca^{2+} ions, although the evidence is not strong enough to establish this as a fact.

Residue-wise RMSD data for the E80:E417 pair in column D of Fig. 5 *a* shows large deviations in both the all-charged systems (2 and 5,), where E80 of one monomer flips outward, which is discernible from the final snapshots of these systems shown in Fig. 5 *c*. The chamber widens in both simulations, although it narrows back quickly in system 2 when the cations fill in. The uncharged system 3 remains close to the starting structure, whereas the charged-uncharged system 4, although designed to mimic the crystal structure, shows appreciable deviation, with E80 flipping out in one monomer and the chamber widening.

In system 2, the inner chamber and its ions do not have direct access to the mouth of the channel pore. However, chamber widening in the Ca^{2+} system makes the chamber somewhat accessible to the TM pore, indicating the ease with which the chamber and channel pore could communicate. Another observation during the simulations was that Na^+ ions very rarely entered the V-shaped windows (Fig. 1) or visited the polar and acidic residues located near the entrance of the channel pore, even though these windows appear to be an easy route for ions to reach the pore as has been proposed previously (14). This behavior is observable in the cation binding data for residues E426 and D433 (Fig. 6 *a*), which are located at the TM pore entrance, and proposed to be Ca^{2+} binding sites in previous studies (10). The reason for this behavior appears in the electrostatic potential plot for systems 2 and 5, shown in Fig. 6 *b*, where a positive potential, which is observable at the outer edges of the windows, is caused by the heavy presence of positively charged residues in this region (Fig. 1). This positive potential presents a barrier against the approach of cations to this surface, hence constricting the path through which a cation can access the pore. These observations, coupled with the proximity of the chamber to the pore, hint that the inner chamber might serve as a temporary reservoir of Na^+ ions that are released to the channel pore when it opens, possibly providing an alternate path for cations to access the pore.

The characteristic features of this site, that is, Na^+ accumulation, Na^+ selectivity over Ca^{2+}, and the possibility of chamber widening observed in different systems, suggest that the E80:E417 pair may be involved in the interaction of Na^+ with ASIC. Experimental mutagenesis studies have previously shown that mutations at positions equivalent to residue E80 in ASIC2a (12) and rat ASIC1a (13) strongly impair channel function, lending further support to our conclusion that the E80:E417 pair plays a significant role in ion permeation and channel gating.

Ca^{2+} induced conformational changes

Five surface residue pairs were observed to bind Ca^{2+} persistently. The protonation states of these residues were not altered during these studies, and they exist as charged acidic residues in all systems. These pairs are E339:E343, D132:E133, and D127:E236 (Fig. 4 *b*, *top panel*) and E299:D332 and D290:E363 (Fig. 4 *b*, *bottom panel*); their corresponding ion binding patterns are shown in columns E–I in Fig. 4 *c*.

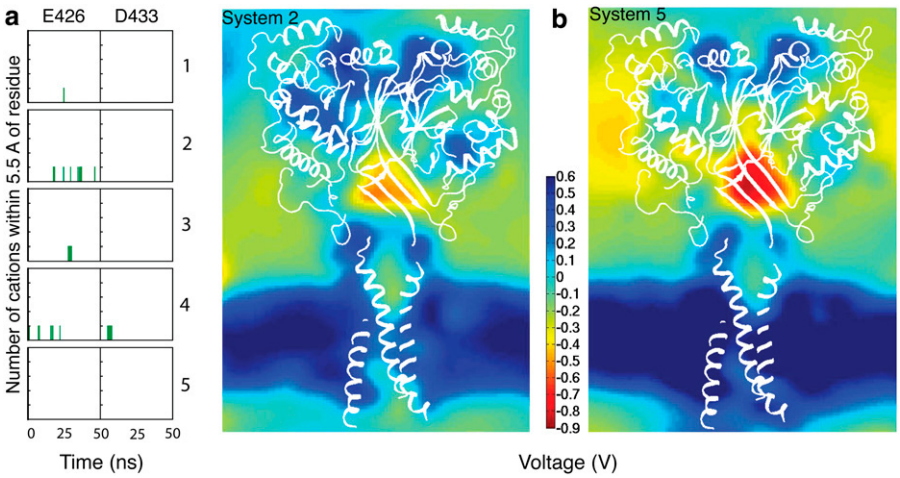

FIGURE 6 (*a*) Cation binding at residues E426 and D433 located at the entrance of the TM pore. (*b*) A slice of the electrostatic potential surface averaged over the trajectories for system 2 and 5, respectively. The slice, taken parallel to the axis of the protein and at the V-shaped windows, shows high negative potential (*red*) in the inner chamber and positive potential at the edges of the V-shaped windows (*blue*).

Although Na^+ binding is observed at these five sites, it is much less persistent than Ca^{2+} binding in most cases. The cation binding patterns for Ca^{2+} (system 5) show that sites D132:E133 and D127:E236 persistently bind one Ca^{2+} ion, whereas E339:E343, E299:D332, and D290:E363 persistently bind one to two Ca^{2+} ions each. Especially notable are the D127:E236, E299:D332, and D290:E363 pairs in which the constituent residues are too distant (~8–18 Å) in the crystal structure to form a pair but exhibit Ca^{2+}-induced binding and pair formation.

Residue-wise RMSDs indicate that the residues in all five pairs described above show significant deviation from the starting structure in all systems (Fig. 5 *a*, *columns E–I*), because they are mostly located on mobile loops in the structure (Fig. 4 *b*). However, a closer examination of these structural transitions reveals a striking difference between the Na^+ and the Ca^{2+} systems. In system 1 through 4, these deviations result mainly from random side-chain fluctuations. In system 5, however, the side-chain movement is directional in three of these five residue pairs and the carboxylic carbons of the D127:E236, E299:D332, and D290:E363 pairs are at a distance of ~18 Å, ~11 Å, and ~8 Å, respectively, in the starting structure. During the simulation, however, these pairs orient toward each other and move by ~5 to15 Å closer to form a Ca^{2+} binding pair. This motion is associated with significant slanting of the thumb domain (Fig. 1), which is a structural domain in ASIC1 highlighted by four disulphide bridges formed from highly conserved cysteine residues and is believed to play an important role in channel gating (14). This movement is visible in the structural overlays shown in Fig. 5 *d*. Thus, these observations suggest a possibly significant role of the D127:E236, E299:D332, and D290:E363 pairs as acid sensing sites where substitution of Ca^{2+} by H^+ could cause conformational changes associated with channel gating.

Experimental mutagenesis studies have been reported for the rat ASIC1 system at positions equivalent to three residues of these pairs, namely, E236, E299, and E343 (13). Mutation of E236 does not decrease the H^+ activated current, suggesting that the D127:E236 pair may not be involved in acid activation; however, it may be involved in channel inhibition caused by Ca^{2+} binding. Mutations of E299 and E343 show a decrease in H^+ activated current, thus providing further support for a possible role for the E299:D332 and E339:E343 pairs in acid sensing. Consolidating our results from cation binding data, structural deviations, and those results reported in experimental studies, we conclude that E299:D332, E339:E343, and D290:E363 pairs are strong candidates for acid (H^+) sensing sites.

Cation binding to the TM domain

The three E451:D454 pairs at the cytosolic end of the TM region form a ring of acidic residues that binds Na^+ ions intermittently but binds Ca^{2+} persistently throughout the simulations (Fig. 4 *c*, *column J*). We do not consider it to be a possible acid sensing site, because it is known that acid sensing occurs on the periplasmic side. However, persistent cation binding draws attention toward this site. Na^+ binding is negligible in systems 1 and 2, but it is relatively persistent in systems 3 and 4, where sometimes more than one Na^+ ion binds. One Ca^{2+} cation is observed to be bound throughout the simulation at this site. The observation of persistent Ca^{2+} binding at the E451:D454 pair might have low physiological relevance considering that $[Ca^{2+}]$ in this simulation system is ~50 mM, which is much higher than the physiological intracellular $[Ca^{2+}]$. However, Na^+ binding to this site might play a role in the mechanism and rate of ion permeation through the pore.

Sequence analysis supports proposed candidates for acid sensing

The functional relevance of the 10 residue pairs studied was examined based on comprehensive sequence alignment data reported in the Supplementary Material of the study by Jasti and colleagues (14) that compared 32 sequences from several species, including all ASIC subtypes and three other members of the DEG/ENaC sodium channel family, namely, FaNaCh, ENaCα, and MEC-4, which are H^+ insensitive. The six ASIC subtypes (ASIC1a, ASIC1b, ASIC2a, ASIC2b, ASIC3, and ASIC4) differ in their H^+ sensitivities and activation and desensitization patterns (4). ASIC2b and ASIC4 are H^+ insensitive when expressed alone and are functional only as heteromultimers with other subtypes. It is reasonable to assume that this difference in H^+ sensitivity among subtypes is due to differences in the composition of acid sensors. Therefore, sequence comparison among these subtypes can provide more clues about the H^+ sensors.

TABLE 3 Conservation of residue pairs in the six ASIC subtypes based on sequence comparison data (14)

Subtype	D238:D350	E239:D346	E220:D408	E80:E417	E339:E343	D132:E133	D127:E236	E299:D332	D290:E363	E451:D454
ASIC1a	C	C	C	C	C	C	C	C	C	C
ASIC1b	C	C	C	C	C	C	N	C	C	C
ASIC2a	n	C	C	C	C	n	C	C	n	C
ASIC2b	n	C	C	n	C	C	C	C	n	C
ASIC3	C	n	C	C	n	n	N	n	n	C
ASIC4	n	C	C	C	n	n	N	n	n	C

If both residues in a pair are conserved, the pair is designated by ''C'' (conserved), whereas if any one residue of the pair is not conserved, the pair is designated as ''n'' (not conserved).

The results of this analysis are summarized in Table 3. A residue pair was considered as conserved only if both the constituent acidic residues were conserved. Based on this criterion, each residue pair was classified as conserved (C) or not conserved (n) in Table 3 across a particular subtype. Among the acidic pocket pairs, the D238:D350 pair is conserved only in ASIC1a, ASIC1b, and ASIC3, which also are the most sensitive among the ASIC subtypes. The E239:D346 pair is conserved in all ASICs except ASIC3. E220:D408 is strongly conserved throughout ASICs. The inner chamber residue pair E80:E417 is conserved across almost all ASICs except in the H^+ insensitive ASIC2b. Among the Ca^{2+} binding surface residue pairs (E339:E343, D132:E133, D127:E236, E299:D332, and D290:E363), all five pairs may act as acidic pairs in ASIC1a, whereas none of these can assume this role in ASIC3 or ASIC4. Also, E339:E343, D127:E236, and E299:D332 may form acidic pairs in ASIC2a and ASIC2b.

Based on these observations, it may be concluded that, although some putative acid sensing sites are common among all ASICs (E80:E417 and E220:D408), those that are not common are responsible for modulation of the pH sensitivity of the channel. Thus, it appears that the higher H^+ sensitivity of ASIC1a compared to ASIC3 is possibly due to the E239:D346 pair in the acidic pocket and the five Ca^{2+} binding surface residue pairs; all of these pairs are present in ASIC1a but absent in ASIC3. Similarly, ASIC3 is probably more pH sensitive than ASIC2a due to the presence of the D238:D350 acidic pocket pair, despite ASIC2a carrying three Ca^{2+} binding surface residues that are absent in ASIC3. Also, the absence of the E80:E417 pair in ASIC2b might relate to its H^+ insensitivity, whereas insensitivity in ASIC4 might be due to the combined effect of the absence of the D238:D350 pair and all of the five Ca^{2+} binding surface residue pairs.

None of these nine residue pairs discussed above are conserved (by our definition as described above) in the FaNach, ENaCα, or MEC-4 channels. This finding suggests that these channels might play a functional role only in ASICs, thus supporting the possibility of their role as acid sensors. The observation that these pairs are not present throughout all ASIC subtypes suggests that the presence or absence of these pairs, or one of the pair's constituent residues, may modulate the H^+ sensitivity of the subtypes as discussed above. The TM region acidic pair E451:D454 is highly conserved throughout ASICs, as well as in the FaNach, ENaCα, or MEC-4 channels, supporting our hypothesis that there is a common functional role for E451:D454 in this Na^+ channel family.

CONCLUSIONS

A series of molecular dynamics simulations were performed on the ASIC1 system at different protonation states and in the presence of either Na^+ or Ca^{2+} ions to examine potential cation and ligand (H^+) binding sites of the protein. The results reveal several pairs of acidic residues that form sites of cation localization and that could be significant as binding sites for Ca^{2+}, a known modulator of gating, and/or as binding sites for H^+, which activates the channel. The identified residue pairs, therefore, might be directly involved in the channel activation mechanism. Apart from persistent cation binding, most of these residue pairs are associated with appreciable structural changes, hinting at the conformational changes that might occur on the substitution of Ca^{2+} by H^+ at these sites, a proposed mechanism by which H^+ activation occurs.

It has been proposed in previous experimental studies that the H^+ sensor may be distributed over the protein structure. Based on our studies on cation binding and associated structural deviation, as well as some data from experimental studies, we propose that at least 6 of the observed 10 pairs in this study are strong candidates for participation in the acid (H^+) sensing mechanism. These six pairs are D238:D350 and E239:D346 pairs in the acidic pocket; E80:E417 pairs in the inner chamber; and E299:D332, E339:E343, and D290:E363 pairs on the protein surface. This study also provides some details about protein residues that might be involved in structural transitions induced by cation/H^+ binding/unbinding events. Three additional residue pairs among the observed 10 pairs show promise for acid sensing based on the cation binding patterns; however, they are either not associated with significant structural changes (E220:D408 and D132:E133) or not supported by experimental evidence (D127:E236). Analysis of the sequence of ASICs supports the possible involvement of most of these proposed pairs in the acid sensing mechanism.

The dynamics and binding patterns of Ca^{2+} and Na^+ ions around the protein show interesting differences. Na^+ ions access an acidic inner chamber in the protein that Ca^{2+} does not enter. In addition, the chamber may be a temporary reservoir for Na^+ with possible access to the TM pore in the open state of the channel. Ca^{2+} binding also causes three pairs of surface acidic residues, which are initially distant, to move together and form a cation binding pair, an effect that is not observed with Na^+. Other notable structural effects of cation/H^+ binding observed during the simulations include slanting of the thumb domain, widening of the inner chamber, and loop movement in the acidic pocket. The study thus provides several structural and dynamic details associated with ligand (H^+) and cation binding in ASIC1 that might be of relevance to potential acid sensing sites and the mechanism of activation in ASIC1.

SUPPLEMENTARY MATERIAL

To view all of the supplemental files associated with this article, visit www.biophysj.org.

The simulations have been performed using the TERAGRID resources (grant number MCA06N060), the Big Red cluster at Indiana University, and the National Center for Supercomputing Applications Abe cluster, as well as on the Computational Science and Engineering Turing cluster of the University of Illinois at Urbana-Champaign.

REFERENCES

1. Garcia-Anoveros, J., B. Derfler, J. Neville-Golden, B. T. Hyman, and D. P. Corey. 1997. BNaC1 and BNaC2 constitute a new family of human neuronal sodium channels related to degenerins and epithelial sodium channels. *Proc. Natl. Acad. Sci. USA*. 94:1459–1464.
2. Waldmann, R., and M. Lazdunski. 1998. H^+ gated cation channels: neuronal acid sensors in the NaC/DEG family of ion channels. *Curr. Opin. Neurol.* 8:418–424.
3. Kellenberger, S., and L. Schild. 2002. Epithelial sodium channel/degenerin family of ion channels: a variety of functions for a shared structure. *Physiol. Rev.* 82:735–767.
4. Zhang, P., and C. M. Canessa. 2002. Single channel properties of rat acid-sensitive ion channel-1α, -2a, and -3 expressed in *Xenopus* oocytes. *J. Gen. Physiol.* 120:553–566.
5. Hesselager, M., D. B. Timmermann, and P. K. Ahring. 2004. pH Dependency and desensitization kinetics of heterologously expressed combinations of acid-sensing ion channel subunits. *J. Biol. Chem.* 279:11006–11015.
6. Krishtal, O., and V. Pidoplichko. 1980. A receptor for protons in the nerve cell membrane. *Neuroscience*. 5:2325–2327.
7. Waldmann, R., G. Champigny, F. Bassilana, C. Heurteaux, and M. Lazdunski. 1997. A proton-gated cation channel involved in acid-sensing. *Nature*. 386:173–177.
8. Immke, D. C., and E. W. McCleskey. 2001. Lactate enhances the acid-sensing Na^+ channel on ischemia-sensing neurons. *Nat. Neurosci.* 4: 869–870.
9. Immke, D. C., and E. W. McCleskey. 2003. Protons open acid-sensing ion channels by catalyzing relief of Ca^{2+} blockade. *Neuron.* 37:75–84.
10. Paukert, M., E. Babini, M. Pusch, and S. Grunder. 2004. Identification of the Ca^{2+} blocking site of acid-sensing ion channel (ASIC) 1: implications for channel gating. *J. Gen. Physiol.* 124:383–394.
11. Zhang, P., F. J. Sigworth, and C. M. Canessa. 2006. Gating of acid-sensitive ion channel-1: release of Ca^{2+} block vs. allosteric mechanism. *J. Gen. Physiol.* 127:109–117.
12. Smith, E. S. J., X. Zhang, H. Cadiou, and P. A. McNaughton. 2007. Proton binding sites involved in the activation of acid-sensing ion channel ASIC2a. *Neurosci. Lett.* 426:12–17.
13. Paukert, M., X. Chen, G. Polleichtner, H. Schindelin, and S. Grunder. 2008. candidate amino acids involved in H^+ gating of acid-sensing ion channel 1a. *J. Biol. Chem.* 283:572–581.
14. Jasti, J., H. Furukawa, E. B. Gonzales, and E. Gouaux. 2007. Structure of acid-sensing ion channel 1 at 1.9 Å resolution and low pH. *Nature*. 449:316–323.
15. Hui Li, A. D. R., and J. H. Jensen. 2005. Very fast empirical prediction and interpretation of protein pKa values. *Proteins*. 61:704–721.
16. Humphrey, W., A. Dalke, and K. Schulten. 1996. VMD: visual molecular dynamics. *J. Mol. Graph.* 14:33–38.
17. MacKerell, A., Jr., D. Bashford, M. Bellott, R. L. Dunbrack, Jr., J. Evanseck, M. J. Field, S. Fischer, J. Gao, H. Guo, S. Ha, D. Joseph, L. Kuchnir, K. Kuczera, F. T. K. Lau, C. Mattos, S. Michnick, T. Ngo, D. T. Nguyen, B. Prodhom, I. W. E. Reiher, B. Roux, M. Schlenkrich, J. Smith, R. Stote, J. Straub, M. Watanabe, J. Wiorkiewicz-Kuczera, D. Yin, and M. Karplus. 1998. All-atom empirical potential for molecular modeling and dynamics studies of proteins. *J. Phys. Chem. B*. 102: 3586–3616.
18. Stone, J. E., J. C. Phillips, P. L. Freddolino, D. J. Hardy, L. G. Trabuco, and K. Schulten. 2007. Accelerating molecular modeling applications with graphics processors. *J. Comput. Chem.* 28:2618–2640.
19. Phillips, J. C., R. Braun, W. Wang, J. Gumbart, E. Tajkhorshid, E. Villa, C. Chipot, R. D. Skeel, L. Kale, and K. Schulten. 2005. Scalable molecular dynamics with NAMD. *J. Comput. Chem.* 26:1781–1802.
20. MacKerell, A. D., Jr., M. Feig, and C. L. Brooks III. 2004. Extending the treatment of backbone energetics in protein force fields: limitations of gas-phase quantum mechanics in reproducing protein conformational distributions in molecular dynamics simulations. *J. Comput. Chem.* 25:1400–1415.
21. Jorgensen, W. L., J. Chandrasekhar, J. D. Madura, R. W. Impey, and M. L. Klein. 1983. Comparison of simple potential functions for simulating liquid water. *J. Chem. Phys.* 79:926–935.
22. Darden, T., D. York, and L. Pedersen. 1993. Particle mesh Ewald. An N·log(N) method for Ewald sums in large systems. *J. Chem. Phys.* 98:10089–10092.
23. Martyna, G. J., D. J. Tobias, and M. L. Klein. 1994. Constant pressure molecular dynamics algorithms. *J. Chem. Phys.* 101:4177–4189.
24. Feller, S. E., Y. H. Zhang, R. W. Pastor, and B. R. Brooks. 1995. Constant pressure molecular dynamics simulation — the Langevin piston method. *J. Chem. Phys.* 103:4613–4621.